Nanoscale

PAPER

View Article Online
View Journal | View Issue

Cite this: *Nanoscale*, 2024, **16**, 16058

Restoring physiological parameters of the pancreas and kidney through treatment with a polymeric nano-formulation of C-peptide and lisofylline combination in diabetic nephropathy†

Arihant Kumar Singh, Kommera Sai Pradyuth, Deepak Chitkara and Anupama Mittal *

Diabetic nephropathy (DN) is a progressive kidney disorder that develops as a complication of diabetes due to long-term exposure to elevated blood glucose levels (BGLs). In this case, an intervention of therapeutic moieties is needed to target the specific elements involved in diabetes to prevent/delay the deterioration of kidney function. Therefore, the present study focused on designing and evaluating a potent nano-formulation of a combination of C-peptide (CPep) and the anti-diabetic drug lisofylline (LSF) to prevent streptozotocin (STZ)-induced DN. As a strategic intervention, an LSF-oleic acid prodrug (LSF-OA) was initially synthesized and further encapsulated in an in-house-synthesized cationic polymer [(mPEG-*b*-P(CB-{g-DMDP}-*co*-LA)); mPLM] to prepare polymeric nano-complexes of CPep *via* electrostatic interaction, possessing a size of 218.6 ± 14.4 nm and zeta potential of +5.2 mV together with stability for 30 days at 25 °C. mPLM-LSF-OA-CPep nanoparticles demonstrated hemocompatibility with RBCs and exhibited potent anti-oxidant activity by reducing nitrite levels, inducing the release of anti-oxidant GSH and protecting metabolically stressed rat kidneys and murine insulinoma cells from apoptosis. *In vivo* pharmacokinetics depicted an increase in $t_{\frac{1}{2}}$ and mean residence time in rats, which further improved the BGL and renal conditions and reduced plasma IL-6 and TNF-α levels in the STZ-induced DN animal model when treated with mPLM-LSF-OA-CPep compared to free LSF and CPep. Moreover, an increase in the plasma insulin level and detection of proliferative marker cells in pancreatic islets suggested the regeneration of β-cells in diabetic animals.

Received 9th May 2024,
Accepted 17th July 2024

DOI: 10.1039/d4nr02010c

rsc.li/nanoscale

1. Introduction

Diabetes mellitus (DM) and its associated complications are a significant cause of various health risks, including infections, chronic kidney disease (CKD), severe liver disease, cardiovascular issues, stroke, and cancer. Although diabetes management involves preventive measures, lifestyle improvements, strict glycemic control, and management of hypertensive and lipid profiles, complications arising from diabetes are deemed severe and necessitate appropriate medication and rigorous diabetes control. Accordingly, in all instances, the available treatment for diabetic complications, especially diabetic nephropathy (DN), needs more specific treatment options. Besides, the scarcity of treatment options makes this condition incurable, and it becomes difficult to restrict its further advancement.[1,2]

The global prevalence of diabetes is rapidly increasing, particularly in developing countries such as India. Consequently, DN has emerged as a significant contributor to end-stage kidney diseases, accounting for approximately one-third of cases. Presently, the main focus has shifted to CKD treatment *via* both intensified glycaemic control and reduction in high blood pressure.[3,4] Lisofylline (LSF) is a small molecule drug that possesses anti-inflammatory and immunomodulatory effects and has been reported as a treatment intervention for type 1 diabetes mellitus (T1DM) in clinical trials, with the potential to prevent cell death together with the protection and regeneration of pancreatic beta cells.[5] The anti-diabetic activity of LSF is majorly attributed to its ability to (a) inhibit the production of proinflammatory cytokines (IL-1β, TNF-α and IFN-γ) and (b) effectively suppress T-cell activation and differentiation *via* the inhibition of STAT4-mediated IL-12 signaling.[6] Most importantly, LSF can also maintain β-cell insulin secretory function in the presence of inflammatory cytokines

Department of Pharmacy, Birla Institute of Technology and Science (BITS PILANI), Pilani, Rajasthan, 333031, India. E-mail: anupama.mittal@pilani.bits-pilani.ac.in; Tel: +91 1596 515708; Mobile: +91 9660876009

† Electronic supplementary information (ESI) available. See DOI: https://doi.org/10.1039/d4nr02010c

and regulate immune cell function to suppress autoimmunity. However, LSF is associated with formulation challenges due to its physicochemical properties, including high aqueous solubility (~60 mg mL^{-1} in water), which hinders its encapsulation in delivery systems, and short biological half-life ($t_{\frac{1}{2}}$). LSF has been reported to be orally non-bioavailable and needs to be administered at a high dose of 25 mg kg^{-1} twice daily in T1D animals and in clinical trials, at a single dose of 12 mg kg^{-1} by continuous subcutaneous (s.c.) or i.v. infusion over 24 h.[7] It also undergoes rapid metabolism to form metabolite PTX and this LSF-PTX interconversion is mainly responsible for the high dose of LSF.[8] Thus, to overcome the barriers associated with the effective delivery of LSF, our lab developed a drug-fatty acid conjugate. These conjugates were synthesized through an esterification reaction, aiming to enhance the pharmacokinetic performance of LSF. Among the different prodrugs synthesized and reported by our lab, LSF-oleic acid (LSF-OA) exhibited the most promising *in vitro* and *in vivo* performance.[9] Recently, a combination of LSF (27 mg kg^{-1} day^{-1}) was reported with exendin-4 (Ex-4; 18 nM day^{-1}) to be administered subcutaneously by Alzet osmotic minipumps to facilitate its stable systemic delivery over fourteen days. The specific underlying mechanism for the synergistic action of LSF and exenatide-4 was not very clear, but LSF enhanced the mitochondrial activity and prevented STAT-4 activation in tissues of interest, whereas Ex-4 acted as an activator of the GLP-1 receptor by inducing cyclic AMP and protein kinase A stimulation.[10]

Another potent anti-diabetic molecule is C-peptide (CPep), which plays a renoprotective role by suppressing the TGF-β pathway and exhibits anti-apoptotic activity, thus imparting significant improvement in the microvascular system together with controlling the glomerular filtration rate (GFR).[11] It also shows anti-inflammatory activity, and therefore demonstrated a decrease in the cytokine levels in DN models. CPep is a polypeptide composed of 31 amino acids, which was initially identified as a cleaved subunit of proinsulin. However, it is now well-known for its ability to mitigate microvascular complications in diabetes-induced kidney disorders due to its prominent anti-inflammatory effects.[12] Nevertheless, despite these therapeutic benefits, CPep encounters challenges in terms of its formulation including low stability, limited circulation half-life (30 min), and rapid elimination. Recently, nanotechnology has emerged as a promising avenue to overcome the limitations associated with peptide delivery including CPep as a therapeutic molecule.[13,14] In a 12-month clinical trial, the efficacy of PEGylated CPep was evaluated in the context of peripheral neuropathy in T1D microvascular complications and compared with native CPep. Among 250 patients with T1D and peripheral neuropathy who received a weekly dose ranging from 0.8 to 2.4 mg for 52 weeks, an improvement in the vibration perception threshold (VPT) was noted.[15] In a separate study, Jun Lee *et al.* reported the development of a K9-C-peptide hydrogel formulation designed to mitigate hyperglycemia-induced vascular dysfunction, including ROS generation, inflammation, and apoptosis in the aorta of diabetic mice. This formulation based on elastin-like polypeptide conjugation with CPep achieved a sustained release of CPep over 19 days. Also, the hydrogel demonstrated the capability to restore diabetic aortic dysfunction.[16]

This presents a strong rationale to design a co-delivery system for LSF and CPep for the treatment of DN. In this case, LSF is anticipated to manage the diabetic condition, while CPep is expected to contribute to kidney protection. Herein, we combined the therapeutic advantages of the LSF-OA prodrug with CPep by co-delivering them using an in-house-synthesized high molecular weight cationic polymer. The strategy involved the encapsulation of LSF-OA inside polymeric nanoparticles, followed by its lyophilization, and then complexation of CPep by electrostatic interaction. The combination formulation was further evaluated for its anti-oxidant, anti-apoptotic and proliferative activities on metabolically stressed kidney and insulinoma cells. After screening the nanoparticles for hemocompatibility, their pharmacokinetic profile was also generated and compared with our previously published data for free LSF and LSF-OA[9] and CPep nano-complexes.[17] The efficacy of the combination delivery was further evaluated for its effect on pancreatic islets and diabetic kidney complications in a streptozotocin (STZ)-induced DN model in Wistar rats.

2. Materials

LSF (purity > 98%, HPLC) and LSF-OA prodrug (purity > 96.5%, HPLC) were synthesized in house.[9] CPep was custom-synthesized and procured from LifeTien, NJ, USA. 3-Isobutyl-1-methylxanthine (IBMX as internal standard; HPLC ≥99%), *N*,*N*-dimethyldipropylenetriamine (DMDP), 3-[4,5-dimethylthiazol-2-yl]-2,5-diphenyltetrazolium bromide (MTT) and methoxy poly(ethylene glycol) (mPEG; 5000 Da) were purchased from Sigma Aldrich (St Louis, MO). 4-Dimethylaminopyridine (DMAP), ethylenediamine tetraacetic acid (EDTA), benzyl bromide and *N*-(3-dimethylaminopropyl)-*N*-ethylcarbodiimide hydrochloride (EDC·HCl) were procured from Spectrochem Ltd (Mumbai, India). STZ was purchased from MP biomedicals LLC, Germany. Trifluoroacetic acid (HPLC grade), sulphanilamide and reduced glutathione (GSH) were purchased from SRL Pvt. Ltd (India). Pentoxifylline (PTX), *N*,*N*-diisopropylethylamine (DIPEA) and D,L-lactide were purchased from TCI chemicals, Japan. Alexa Fluor 488 was purchased from Invitrogen, USA. OA was purchased from Acme Synthetic Chemicals (Mumbai, India). Dulbecco's modified Eagle's medium (DMEM), fetal bovine serum (FBS), rat interleukin-6 (IL-6) and tumour necrosis factor-α (TNF-α) mini ABTS ELISA development kit (PeproTech) were purchased from Thermo Fisher Scientific, USA. The Rat CPep ELISA kit was procured from FineTest (China). All other chemicals and reagents were of analytical grade. MIN-6 and NRK-52E cells were procured from NCCS, Pune (India). The animal protocol has been approved by the Institute Animal Ethical Committee (IAEC) (protocol number IAEC/RES/28/17).

3. Methods

3.1 Synthesis and characterization of LSF-OA prodrug

As reported earlier by our group, LSF was synthesized using PTX *via* a single-step reaction with $NaBH_4$ in the presence of a protic solvent (methanol).[18] It was characterized by HPLC (Shimadzu, Japan) and ^{1}H NMR, 400 MHz (Bruker, Germany). Further, to prevent the conversion of LSF into PTX and to make LSF hydrophobic, it was converted to LSF-OA prodrug, as reported earlier.[9] Subsequently, the prodrug was characterized by ^{1}H NMR and HPLC-based analytical method.

3.2 Synthesis and characterization of cationic polymer (mPEG-*b*-poly(carbonate-{grafted-DMDP}-*co*-lactide))

To facilitate the co-delivery, stability and sustained release of the drug and peptide, a multi-step polymer synthesis was carried out in-house, as reported earlier by our group.[19] The cationic chain (DMDP) was grafted to the free carboxyl pendent groups present on the polymer backbone to synthesize the final copolymer [(mPEG-*b*-P(CB-{g-DMDP}-*co*-LA)); mPLM]. The polymer was characterized by ^{1}H NMR for estimating its molecular weight by determining the number of units of each monomer present in the polymer.

3.3 Preparation of LSF-OA-loaded polymeric nanoparticles (mPLM-LSF-OA)

The nano-formulation of LSF-OA was prepared *via* the single emulsion evaporation method. The cationic polymer and LSF-OA prodrug were dissolved in DCM, followed by probe sonication in 1% Tween 80 aqueous solution at 25% amplitude for 2 min under cold conditions to form the primary emulsion. To solidify the particle surface, the organic solvent was removed from the formulation under vacuum. Any micron sized particles were separated from the formulation by centrifugation at 5000 rpm for 5 min at 4 °C. Further, LSF-OA nanoparticles (mPLM-LSF-OA) were obtained by ultracentrifugation (Sorvall MX150+, Thermo Scientific), and the nanoparticle pellet was redispersed in deionized water. Further, the particle size and zeta potential were measured using a Litesizer (Anton Paar, Austria) and the entrapment efficiency and drug loading were calculated using eqn (1) and (2), respectively.

$$\text{Encapsulation efficiency}(\%\text{EE}) = \frac{\text{Weight of entrapped drug}}{\text{Weight of drug initially taken}} \times 100 \quad (1)$$

$$\text{Drug loading}(\%\text{DL}) = \frac{\text{Weight of entrapped drug}}{\text{Weight of lyophilized nanoparticles}} \times 100 \quad (2)$$

3.4 Lyophilization parameters

Trehalose and PEG 2000 at a concentration of 5% and 10%, respectively, were screened as cryoprotectants for mPLM-LSF-OA and the lyophilized product was analyzed to determine its particle size and zeta potential. Both cryoprotectants were freshly prepared by mixing with the mPLM-LSF-OA formulation and placed inside a batch lyophilizer (Freezone Triad System, LABCONCO, USA). The employed lyophilization parameters and RAMP cycles were optimized by our lab earlier.[20] The lyophilization efficiency was assessed by determining the S_f/S_i ratio for each sample, where S_f represents the particle size after lyophilization and S_i represents the particle size before the freezing cycles. The samples with an S_f/S_i ratio within the range of 1 ± 0.3 were chosen for subsequent studies.[21]

3.5 Preparation of mPLM-LSF-OA-CPep nanoparticles

For complexation, the mPLM-LSF-OA nanoparticles were incubated with CPep for 1 h at RT. Complexation between CPep and mPLM-LSF-OA occurred by electrostatic interaction at neutral pH, wherein CPep attained a negative charge above its isoelectric pH 3.0, while mPLM-LSF-OA was positively charged owing to the presence of a cationic chain on the polymer backbone to achieve the CPep-complexed polymeric LSF-OA nanoparticles (mPLM-LSF-OA-CPep), as illustrated in Fig. 1A. After incubation, the uncomplexed peptide was separated *via* ultracentrifugation at 40 000 rpm for 20 min. The particle size, zeta potential and complexation efficiency (by indirect method using eqn (3)) were evaluated by DLS and HPLC.

$$\%\text{Complexation efficiency} = \frac{\text{Initial concentration of CPep} - \text{concentration of CPep in supernatant}}{\text{Initial concentration of CPep}} \times 100 \quad (3)$$

3.5.1 Complexation efficiency by direct method: heparin competition assay. The competition assay was performed to analyze the amount of CPep complexed with the cationic mPLM-LSF-OA nanoparticles using heparin, which is known to carry a polyanionic charge and used as a competitor to release the complexed peptide from the cationic system.[22] Different concentrations of heparin (0.01 to 10 IU mL^{-1}) were incubated with the mPLM-LSF-OA-CPep nanoparticles in deionized water at RT for 1 h. After incubation, the particles were collected and analyzed by DLS, whereas the CPep released from the complexes was quantified by HPLC.

3.6 Stability study

The benchtop stability study of the mPLM-LSF-OA-CPep nanoparticles was performed to determine the integrity of the nanoparticles in deionized water at 25 °C for 30 days. The nanoparticles were analyzed for their particle size and zeta potential by DLS.

3.7 Hemocompatibility study

Using a method previously reported by our group, the *in vitro* interaction between the nanoparticles and RBCs was investigated.[9] The mPLM-LSF-OA and mPLM-LSF-OA-CPep nanoparticles were dispersed in 1 mL of RBC suspension with negative and positive control groups (normal saline and 0.1%

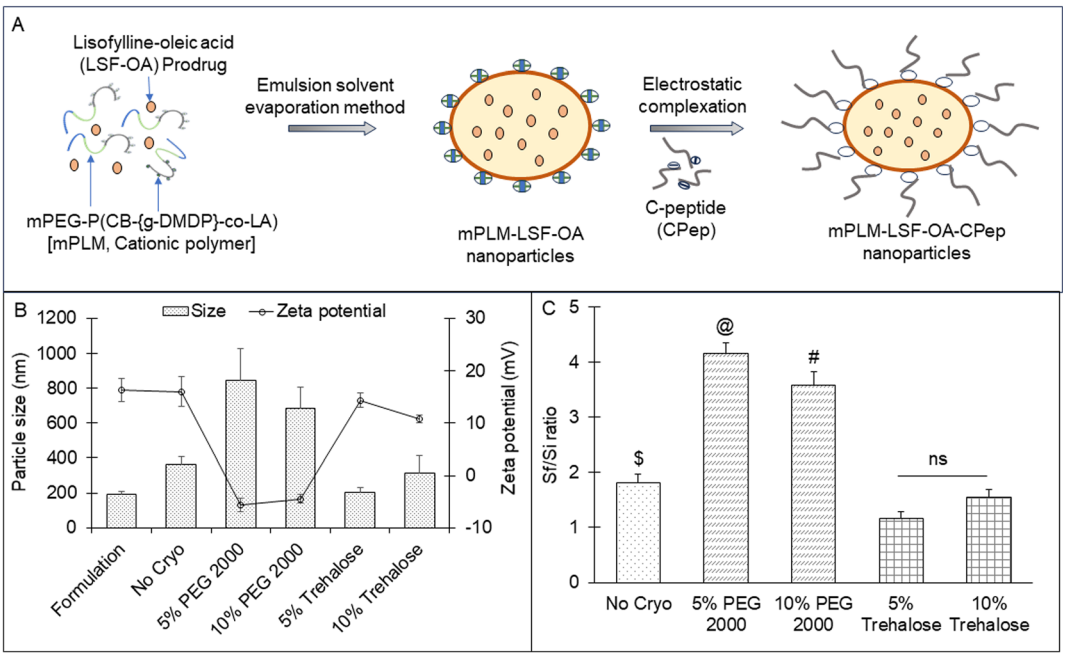

Fig. 1 (A) Schematic of the process to formulate mPLM-LSF-OA-CPep nanoparticles. Screening of a suitable cryoprotectant *via* the characterization of lyophilized mPLM-LSF-OA nanoparticles for (B) size distribution and zeta potential and (C) S_f/S_i ratio studies, where $^{\$}$no cryo *vs.* 5% trehalose ($^{\$}p < 0.01$), $^{@}$5% PEG 2000 *vs.* no cryo, 5% trehalose and 10% trehalose; $^{\#}$10% PEG 2000 *vs.* no cryo, 5% trehalose and 10% trehalose ($^{@\#}p < 0.0001$). Each data point represents mean (n = 3) ± SD. No Cryo: formulation without cryoprotectant, S_f: particle size after lyophilization, and S_i: particle size before freezing cycle.

Triton X solution). After 1 h of incubation at 37 °C, the samples were centrifuged at 2000 rpm for 5 min and their supernatant was analyzed using an Epoch microplate spectrophotometer (BioTek Instruments, VT) to determine their optical density (OD) at 540 nm. Further, % hemolysis was calculated using eqn (4). Also, FESEM analysis of RBCs was performed to understand the morphological changes that occurred due to incubation with various test samples. The RBCs were smeared on coverslips after fixing with paraformaldehyde solution in a 1 : 1 ratio. The cells were dehydrated in ethanol at concentrations ranging from 30% to 100% and dried overnight. The samples were prepared by sputtering with gold on their surface, followed by FESEM analysis.

$$\%\,\text{Hemolysis} = \frac{\text{OD}_{\text{Sample}} - \text{OD}_{\text{Negativecontrol}}}{\text{OD}_{\text{Positivecontrol}} - \text{OD}_{\text{Negativecontrol}}} \times 100 \quad (4)$$

3.8 Cell culture study

To evaluate the efficiency of the mPLM-LSF-OA and mPLM-LSF-OA-CPep nanoparticles under hyperglycemic conditions, MIN-6 and NRK-52E were employed. The cells were cultured in DMEM media supplemented with 10% FBS and 1% antibiotic solution and incubated at 37 °C in a humidified atmosphere with 5% CO_2.

3.8.1 Cell viability study in metabolic stressed cells. The study was performed on two different cells, MIN-6 and NRK-52E, representing pancreatic and kidney cells, respectively. In a 96 well plate, approximately 5 × 10^3 cells were seeded and allowed to adhere overnight. The cytoprotective effect of the treatment groups of mPLM-LSF-OA and mPLM-LSF-OA-CPep was evaluated on the cells under metabolic stress condition. The metabolic stress was induced by exposing the cells to medium containing high glucose (HG; 100 mM dextrose) for 24 h. After stress induction, the medium was replaced with fresh medium containing mPLM-LSF-OA (40 μM LSF-OA) and mPLM-LSF-OA-CPep (40 μM LSF-OA and 50 nM CPep) nanoparticles and the cells were incubated for another 48 h. Using the MTT assay, the percentage of viable cells was analyzed using eqn (5).

$$\%\,\text{Cell Viability} = \frac{\text{OD of the treatment group}}{\text{OD of the control group}} \times 100 \quad (5)$$

3.8.2 Anti-oxidant effect under high glucose-mediated metabolic stress. To assess the anti-oxidant impact of LSF, CPep and both in the combination treatment groups, namely mPLM-LSF-OA and mPLM-LSF-OA-CPep nanoparticles, a comprehensive analysis at the cellular level was conducted using the appropriate methods. Post cell adhesion, the cells were incubated in phenol red-free media containing dextrose (100 mM) for 24 h, followed by treatment for the next 48 h. The conditioned medium was collected from each well separately and centrifuged at 5000 rpm for 5 min to eliminate cellular components for the NO and GSH assays. This was followed by harvesting and washing of the cells with PBS for the apoptosis assay.

3.8.2.1 GSH assay. GSH is an anti-oxidative marker, which was used to confirm the anti-oxidant effect of the treatment groups on metabolically stressed MIN-6 and NRK-52E cells. It serves as an antioxidant and is employed to alleviate the damage caused by ROS. 5,5′-Dithiobis-(2-nitrobenzoic acid) (DTNB), commonly known as Ellman's reagent, reacts with GSH in the medium, forming a yellowish-coloured adduct (GSH-TNB adduct). In this procedure, 100 μL of the prepared cell lysate and conditioned medium were incubated with an equal volume of DTNB solution at 37 °C for 30 min, and subsequently the absorbance was measured at 412 nm using a microplate reader.

3.8.2.2 Nitrite estimation. ROS serves as an oxidative marker produced during intense protein metabolism when cells are under significant stress. Therefore, a reduction in nitrite levels signifies the anti-oxidative impact of the above-mentioned treatment groups. For this assay, Griess reagent, comprised of 1% *p*-amino-benzene sulphonamide and 0.01% naphthylethylenediamine in 2.5% v/v phosphoric acid, was freshly prepared and stored at 4 °C in the dark. Subsequently, 100 μL of the above-collected conditioned medium was combined with 100 μL of Griess reagent and incubated for 30 min. Following incubation, the absorbance was measured at 540 nm using a microplate reader. The concentration of nitrite in the medium was determined by using a previously established standard curve of sodium nitrite.

3.8.2.3 Apoptosis assay. Cells undergo apoptosis under metabolic stress conditions, and therefore this experiment was performed to quantify the extent of apoptosis induced by high glucose and evaluate the protection rendered by the treatment groups. The cells were centrifuged and resuspended in 1× binding buffer and stained with FITC-labeled Annexin V (Annexin-FITC conjugate) for 20 min in a dark room, followed by the addition of propidium iodide. The cells were analyzed using a flow cytometer (Beckman Coulter, USA) and the data were analyzed by CytExpert software.

3.9 Pharmacokinetic study

Previously, our group reported a PK profile for free LSF and its prodrug LSF-OA at a dose of 30 mg kg^{-1} (~15 mg kg^{-1} LSF).[7,9] The PK analysis of the mPLM-LSF-OA nanoparticles was performed at the dose of 30 mg kg^{-1} LSF-OA and mPLM-LSF-OA-CPep nanoparticles at a dose of 30 mg kg^{-1} LSF-OA with 1 μg kg^{-1} dose of CPep in Wistar rats (200 ± 20 g). After the i.v. administration of nanoparticles, blood samples were withdrawn from the retro-orbital plexus at preset time points of 15, 30 min, 1, 2, 4, 8, 12, 24, 48, 72, and 96 h. Centrifugation was used to extract the plasma at 7000 rpm for 5 min, which was stored at −80 °C for further examination. For the determination of the LSF concentration in the plasma aliquots, a simple liquid–liquid extraction (LLE) method was used. The sample was prepared with 100 μL of plasma and 50 μL IS (IBMX, 2 μg mL^{-1}) extracted by dichloromethane, vortexed, centrifuged and evaporated overnight at 40 °C. The residue was reconstituted with 100 μL of mobile phase and examined by the previously reported HPLC method. Briefly, LSF and IBMX were analysed with 80 μL injection volume on the stationary phase, an Inertsil ODS C18 column (250 × 4.6 mm, 5 μm) with methanol : water (1 : 1 v/v) as the mobile phase run in isocratic mode at a flow rate of 1 mL min^{-1} and monitored at a wavelength of 273 nm. Additionally, a commercially available CPep ELISA quantification kit (Rat C-peptide ELISA, FineTest) was used to measure the concentration of CPep in plasma. The plasma concentration-time profile was plotted and analysed by a non-compartmental model approach using Phoenix 8.3 WinNonlin to determine various PK parameters.

3.10 *In vivo* efficacy study

In Wistar rats (200 ± 20 g), an STZ-induced DN model was developed by injecting a single dose of STZ (42 mg kg^{-1}, intraperitoneal injection, i.p.) dissolved in cold citrate buffer (0.01 M, pH 4.5). The fasting blood glucose level (FGL) was determined after 72 h of STZ injection by the tail bleeding method using an Accu-Check active glucometer. Animals with FGL above 250 mg dL^{-1} were considered diabetic and included in the study. After 4 weeks, the animals were randomly divided into four groups including healthy/non-diabetic (NC), diabetic control (DC), diabetic/treated with mPLM-LSF-OA nanoparticles and diabetic/treated with mPLM-LSF-OA-CPep nanoparticles. The animals in the NC and DC groups received sterile saline, while mPLM-LSF-OA and mPLM-LSF-OA-CPep were daily administered with a dose of LSF-OA prodrug (30 mg kg^{-1} day^{-1}) and CPep (1 μg kg^{-1} day^{-1}), respectively, by the i.p. route. The treatment was continued for 4 weeks, where FGL and body weight were measured weekly.

Towards the end of the study (8^{th} week of diabetes), the animals from the DC group started exhibiting apparent renal failure, as confirmed by the renal functional parameters, *i.e.*, albumin and creatinine levels in animal urine. For the urine collection, the rats were housed separately in metabolic cages for 24 h and the volume of urine collected was recorded as mL of urine per 24 h. An increase in these parameters indicated an escalation of DN symptoms and complications. The plasma IL-6 and TNF-α cytokine levels also confirmed the severity of the diseased condition. At the terminal time point, the animal was euthanized. Further, its pancreas and kidney were isolated and stored in 10% formalin solution, processed and stained by H&E, PAS analysis and immunohistochemistry (IHC) with Ki-67 staining.

3.11 Statistical analysis

The *in vitro* data was processed by one-way ANOVA followed by Tukey's multiple comparison test (expressed as mean ± SD). For the animal study, the statistical significance was assessed using one-way ANOVA (followed by Tukey's multiple comparison test using single variance), which was further numerically expressed as mean ± SEM through the use of the Prism 8.0.1 software (GraphPad). The results were considered statistically significant if the *p*-value was <0.05, with the significance levels denoted as **** for $p < 0.0001$, *** for $p < 0.001$, ** for $p < 0.01$ and * for $p < 0.05$.

4. Results

4.1 Synthesis and characterization of LSF-OA prodrug and cationic copolymer

4.1.1. LSF-OA prodrug. LSF with >98% purity was synthesized and characterized by ^{1}H NMR and HPLC (Shimadzu, Japan), followed by the synthesis of the LSF-OA prodrug with >96% purity, 50% yield and characterization by HPLC and ^{1}H NMR. The successful conjugation of OA with LSF was confirmed by the removal of the hydroxyl (–CH–OH$^-$) group proton (at 3.75 ppm) (Fig. S1A†) from LSF and the emergence of an ester group (–CH–COO$^-$) peak at 4.9 ppm in the NMR spectra, signifying the complete absence of free LSF and formation of the prodrug (Fig. S1B†). As reported earlier, the LSF-OA prodrug exhibited an increased retention time R_t = 22.05 min compared to free LSF (R_t = 3.56 min), which is attributed to the enhanced hydrophobicity of the prodrug after conjugation with the fatty acid.

4.1.2. Cationic polymer. For the co-loading of the LSF-OA prodrug and CPep, the cationic copolymer (mPEG-*b*-P(CB-{g-DMDP}-*co*-LA)) was synthesized and its NMR spectrum revealed that the number of monomers attached to the mPLM copolymer was lactic acid = 125 and carbonate units = 78 with 42 units DMDP with a molecular weight of 44 023 Da (Fig. S1C†).

4.2 Preparation and characterization of LSF-OA-loaded polymeric nanoparticles (mPLM-LSF-OA)

The LSF-OA prodrug was encapsulated in the cationic copolymer *via* the single emulsion evaporation method to prepare mPLM-LSF-OA nanoparticles, as shown in Fig. 1A, with an average particle size of 187 ± 10.76 nm (PDI 0.218) and zeta potential of 18.3 ± 2.28 mV in deionized water. Furthermore, the encapsulation efficiency of LSF-OA was found to be 78.89% ± 3.63% with a practical drug loading of 12.20% ± 2.26% in the mPLM-LSF-OA nanoparticles.

4.2.1 Lyophilization of mPLM-LSF-OA nanoparticles. All the lyophilized formulations prepared using PEG 2000 and trehalose (5% and 10% w/v) showed a good appearance with an intact cake. Here, 5% trehalose was found to be better given that it provided a cake with the desired nano-size (203 ± 12.03 nm) and favourable positive zeta potential (14.2 ± 2.20 mV) compared to the lyophilized formulation without cryoprotectant (named no cryo; 363.733 ± 41.71 nm), as illustrated in Fig. 1B. The cakes formed with trehalose were redispersed in less than 30 s compared to PEG 2000 (86 s) and exhibited an adequate S_f/S_i value (1.22), while the other formulations showed S_f/S_i values of more than 1 ± 0.3 (Fig. 1C).

4.3 Preparation of mPLM-LSF-OA-CPep nanoparticles

The lyophilized LSF-OA polymeric nanoparticles were electrostatically complexed with CPep and subjected to analysis by DLS, revealing an average particle size of 208.6 ± 7.4 nm with a PDI of 0.245 ± 0.06 and a zeta potential of 5.2 ± 2.37 mV (Fig. 2A and B, respectively). Interestingly, the mPLM-LSF-OA-CPep nanoparticles exhibited a slightly larger particle size compared to mPLM-LSF-OA. The complexation efficiency of CPep was found to be 82.75%. Furthermore, a reduction in zeta potential was observed due to the process of complexation with negatively charged CPep. A competition assay using

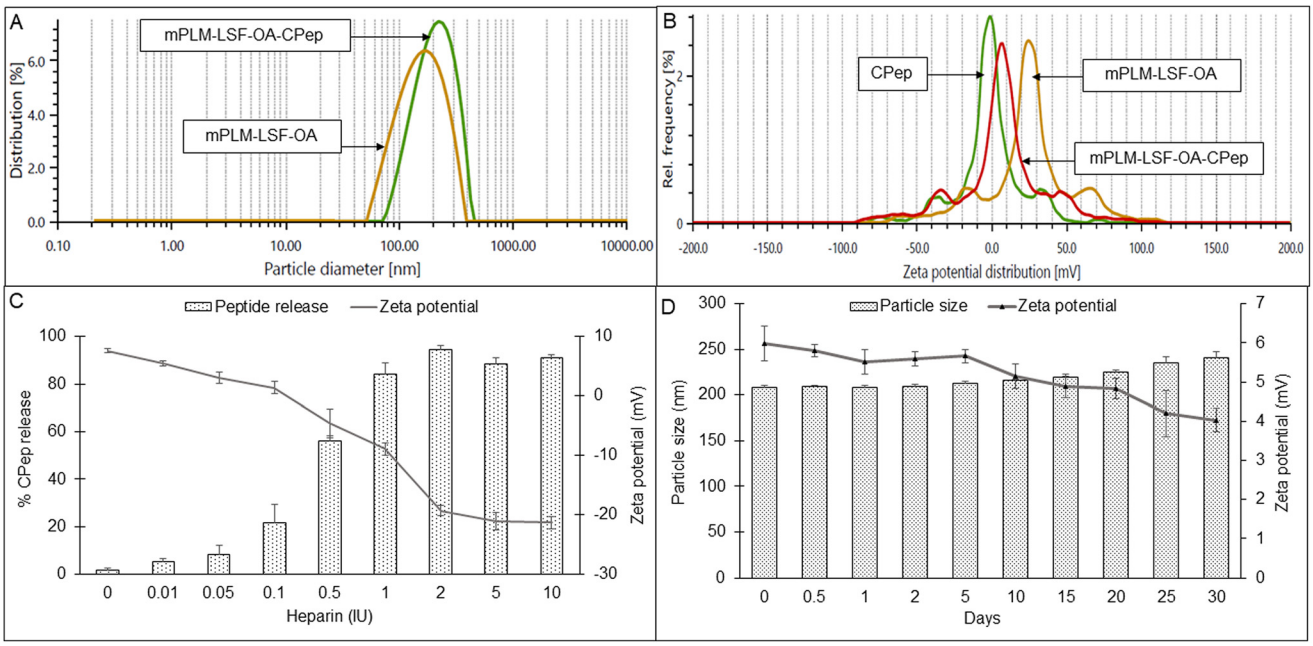

Fig. 2 (A) Size and size distribution and (B) zeta potential of mPLM-LSF-OA and mPLM-LSF-OA-CPep nanoparticles. (C) Heparin competition assay of mPLM-LSF-OA-CPep nanoparticles: % CPep release and zeta potential. (D) Stability study of mPLM-LSF-OA-CPep at 25 °C for 30 days, particle size and zeta potential. Each data point represents mean (n = 3) ± SD.

heparin was conducted to confirm and validate the efficiency of the complexation of CPep with the mPLM-LSF-OA nanoparticles. This assay employed heparin as a competing polyanion to release the complexed CPep (dissociation), which was covalently bound to the surface of the nanoparticles. After the addition of 0.01 IU of heparin to the mPLM-LSF-OA-CPep nanoparticles, CPep started dissociating with a decrease in the zeta potential of the nanoparticles and it continued up to a 2 IU concentration of heparin. Thus, the addition of 2 IU of heparin provided the maximum of ~94% CPep decomplexation from nanoparticles with −19.3 mV zeta potential, as illustrated in Fig. 2C. No further increase in CPep concentration and decrease in zeta potential was observed as the concentration of heparin was further increased up to 10 IU.

4.4 Stability study of mPLM-LSF-OA-CPep nanoparticles

The stability of the mPLM-LSF-OA-CPep nanoparticles was studied at 25 °C for 30 days. As seen in Fig. 2D, after 30 days the particle size was found not to significantly differ from the initial particle size and zeta potential of the nanoparticles.

4.5 Hemocompatibility study

Visual assessment of the integrity of RBCs confirmed the hemocompatibility of the mPLM-LSF-OA and mPLM-LSF-OA-CPep nanoparticles (Fig. 3A). The positive control, containing a potent surfactant (0.1% Triton X), resulted in the lysis of all the RBCs upon incubation for 1 h compared to the other groups. Comparing the OD values of the positive control with the treatment groups, mPLM-LSF-OA and mPLM-LSF-OA-Cep showed minimal hemolysis, *i.e.* 3.64 ± 1.27% and 1.68 ± 0.52% (Fig. 3B and C), respectively.

4.6 Cell culture studies

4.6.1 Cell viability study. In the experiment, metabolic stress conditions were induced in MIN-6 and NRK-52E cells by incubation with HG (100 mM) for 24 h. The MC (under normal glucose) and HG groups were treated as the control groups and some of the HG exposed cells were subsequently treated with mPLM-LSF-OA (LSF-OA: 40 μM) and mPLM-LSF-OA-CPep (LSF-OA: 40 μM, CPep: 50 nM) nanoparticles. Due to the high glucose pretreatment, 34.92% ± 2.13% and 38.17% ± 0.89% cell death were seen in the MIN-6 and NRK-52E cells, respectively. As indicated in Fig. 4, mPLM-LSF-OA resulted in 75.27% ± 1.8% and 75.99% ± 2.83% cell viability under metabolic stress conditions in MIN-6 and NRK-52E, respectively. Interestingly, mPLM-LSF-OA-CPep exhibited 1.08- and 1.16-fold elevated cell viability in metabolic stress-induced MIN-6 and NRK-52E cells in comparison to mPLM-LSF-OA, respectively.

4.6.2 GSH and nitrite assay. Both the insulinoma cells, MIN-6, and kidney cells, NRK-52E, showed reduced GSH production and increased nitrite concentration upon incubation with HG (100 mM)-containing media (Fig. 5A) compared to the control media. This observation clearly indicated the suppression of the anti-oxidative pathways (GSH), resulting in the dominance of oxidative stress (nitrite). Upon treatment with mPLM-LSF-OA, the GSH level increased by 1.62- and 1.27-fold in the MIN-6 and NRK-52E cells, respectively. As shown in

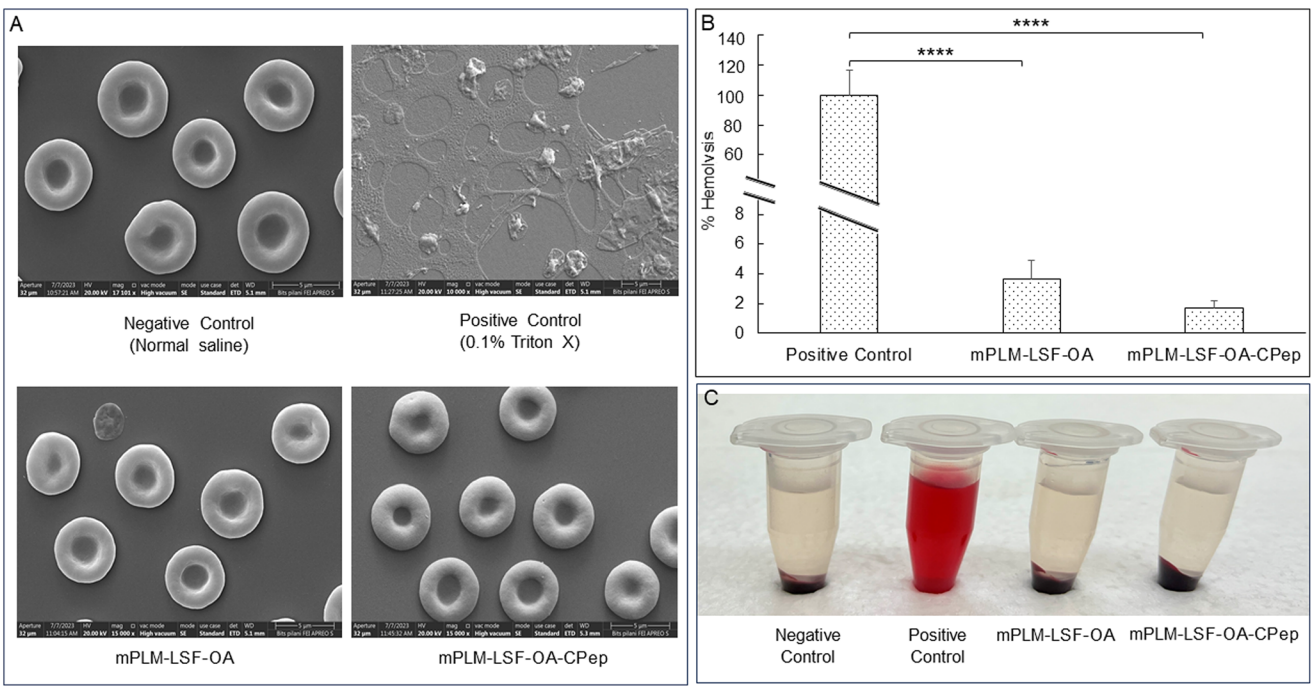

Fig. 3 Hemocompatibility study of mPLM-LSF-OA and mPLM-LSF-OA-CPep nanoparticles. (A) Visual illustration of RBCs after 1 h of incubation with different control and treatment groups using FESEM, (B) hemolysis assay, and (C) digital photograph of hemolysis samples. ****$p < 0.0001$. Each data point represents mean ($n = 3$) ± SD.

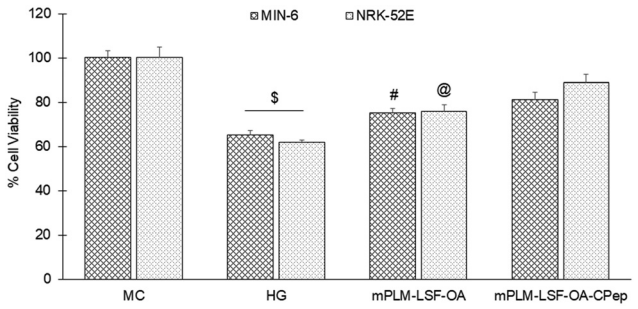

Fig. 4 Cell viability study conducted in metabolic stressed cells, MIN-6 and NRK-52E, after 48 h of treatment, where $^{\$}$HG *vs.* mPLM-LSF-OA and mPLM-LSF-OA-CPep ($^{\$}p < 0.0001$), $^{\#}$mPLM-LSF-OA *vs.* mPLM-LSF-OA-CPep ($^{\#}p < 0.05$), $^{@}$mPLM-LSF-OA *vs.* mPLM-LSF-OA-CPep ($^{@}p < 0.0001$). All data are represented as mean ($n = 3$) ± SD. MC: media control and HG: high glucose.

Fig. 5B, the nitrite concentration was reduced by 1.6- and 1.72-fold in MIN 6 and NRK-52E after treatment with mPLM-LSF-OA, respectively. This elevation of GSH and reduction in nitrite level indicated the reduction of oxidative stress in the presence of the LSF-OA nano-formulation. Comparatively, the combination formulation (mPLM-LSF-OA-CPep) elevated GSH by 2.06- and 1.80-fold with a significant reduction in nitrite concentration to 7.1 ± 1.09 μM and 4.6 ± 0.77 μM in the MIN-6 and NRK-52E cells respectively, clearly demonstrating the synergistic antioxidative effect of CPep in combination with LSF-OA in the treated cells. This study provided evidence of the *in vitro* efficacy of the co-loaded formulation to reduce oxidative stress.

4.6.3 Apoptosis assay. To assess the level of apoptosis induced by hyperglycemic conditioning of the cell media and evaluate the anti-apoptotic activity of the nanoparticles after 48 h of treatment, the Annexin/PI dual-staining technique was employed. In the early stages of apoptosis, Annexin V FITC serves as a probe to quantify the amount of phosphatidylserine on the cell surface due to its high affinity. In the flow cytometry plots depicting FITC-A *vs.* PE-A, four distinct quadrants were identified including lower left (LL – live cells), upper left (UL – necrotic cells), upper right (UR – late apoptotic cells) and lower right (LR – early apoptotic cells), wherein the "apoptotic cells" are accessed by combining the percentage of cells present in the UR & LR quadrants (Fig. 6A). In the MIN-6 cells after 48 h of incubation without treatment, the HG group showed 11.56% of apoptosis, which was reduced by 6.26-fold after treatment with mPLM-LSF-OA-CPep. Consequently, the cells treated with mPLM-LSF-OA developed 4.19-fold higher apoptotic cells than the mPLM-LSF-OA-CPep-treated group. Similarly, the NRK-52E cells after treatment in the mPLM-LSF-OA-CPep group demonstrated a reduction in apoptotic cells by 5.78- and 2.90-fold in comparison to the HG- and mPLM-LSF-OA-treated groups, respectively (Fig. 6B).

4.7 *In vivo* pharmacokinetic study

Non-compartmental analysis of the time *vs.* plasma concentration of LSF and CPep exhibited an improvement in the PK parameters when administered in the form of mPLM-LSF-OA and mPLM-LSF-OA-CPep (Fig. 7A and B). As indicated in Table 1A, mPLM-LSF-OA exhibited a 15.42- and 2.60-fold increase in $t_{\frac{1}{2}}$ in comparison to the free LSF and LSF-OA, respectively. Additionally, the MRT of LSF (in mPLM-LSF-OA)

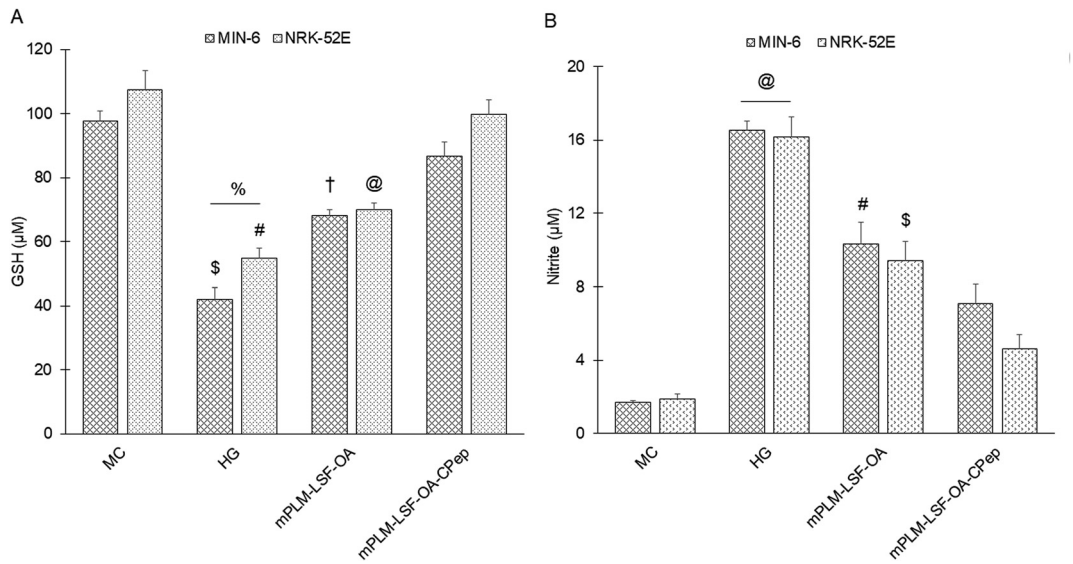

Fig. 5 Comparative estimation of GSH and nitrite levels in the conditioned media of metabolic stressed cells MIN-6 and NRK-52E: (A) GSH, where $^{\%}$HG *vs.* mPLM-LSF-OA-CPep ($^{\$}p < 0.0001$), $^{\$}$HG *vs.* mPLM-LSF-OA ($^{\$}p < 0.0001$), $^{\#}$HG *vs.* mPLM-LSF-OA ($^{\#}p < 0.01$), †mPLM-LSF-OA *vs.* mPLM-LSF-OA-CPep ($^{\dagger}p < 0.001$), $^{@}$mPLM-LSF-OA-CPep *vs.* HG and mPLM-LSF-OA-CPep ($^{@}p < 0.0001$) and (B) nitrite levels, where $^{@}$HG *vs.* mPLM-LSF-OA and mPLM-LSF-OA-CPep ($^{@}p < 0.0001$), $^{\#}$mPLM-LSF-OA *vs.* mPLM-LSF-OA-CPep ($^{\#}p < 0.01$), and $^{\$}$mPLM-LSF-OA *vs.* mPLM-LSF-OA-CPep ($^{\$}p < 0.001$). All data are represented as mean ($n = 3$) ± SD. MC: media control, HG: high glucose, and GSH: reduced glutathione.

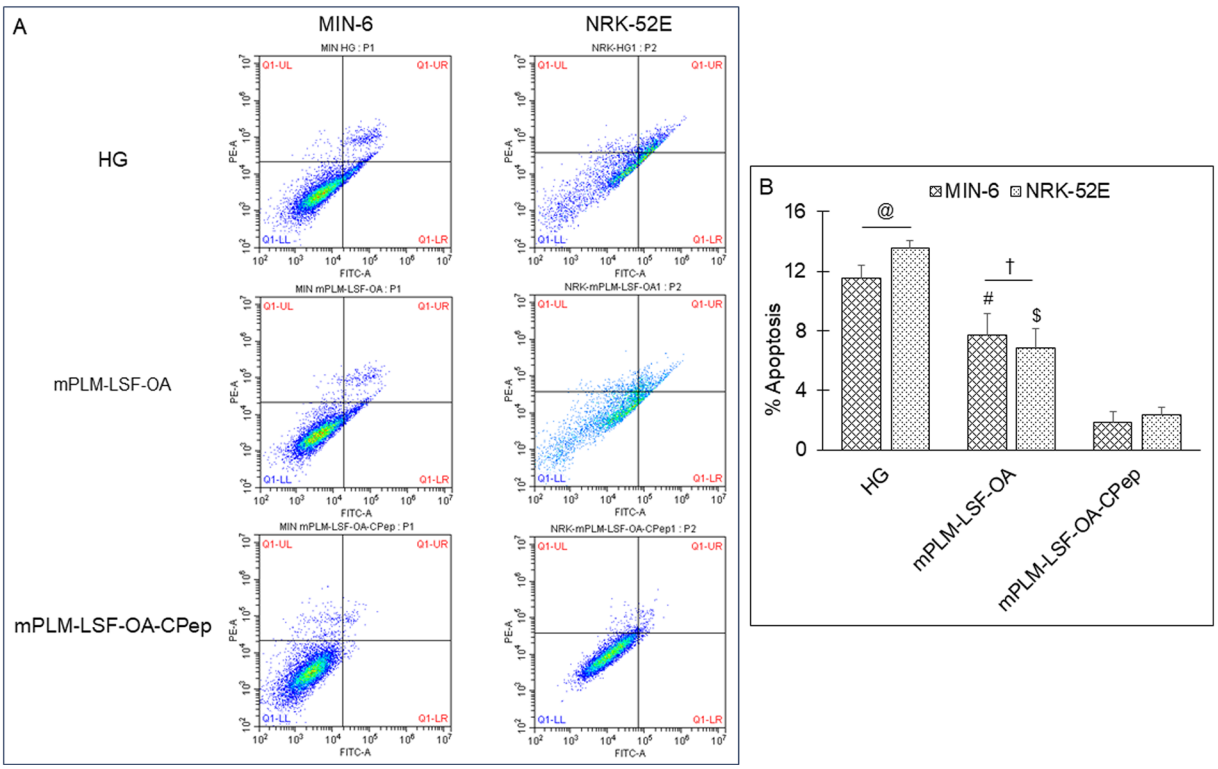

Fig. 6 Annexin V/PI staining of MIN-6 and NRK-52E cells after treatment with mPLM-LSF-OA and mPLM-LSF-OA-CPep for 48 h analysed *via* flow cytometry. (A) Dot plot and (B) % apoptosis. $^{@}$HG *vs.* mPLM-LSF-OA-CPep ($^{@}p < 0.0001$), $^{\#}$mPLM-LSF-OA *vs.* HG ($^{\#}p < 0.05$), $^{\$}$mPLM-LSF-OA *vs.* HG ($^{\$}p < 0.0005$) and, †mPLM-LSF-OA *vs.* mPLM-LSF-OA-CPep ($^{\dagger}p < 0.005$). All data are represented as mean ($n = 3$) ± SD. HG: high glucose.

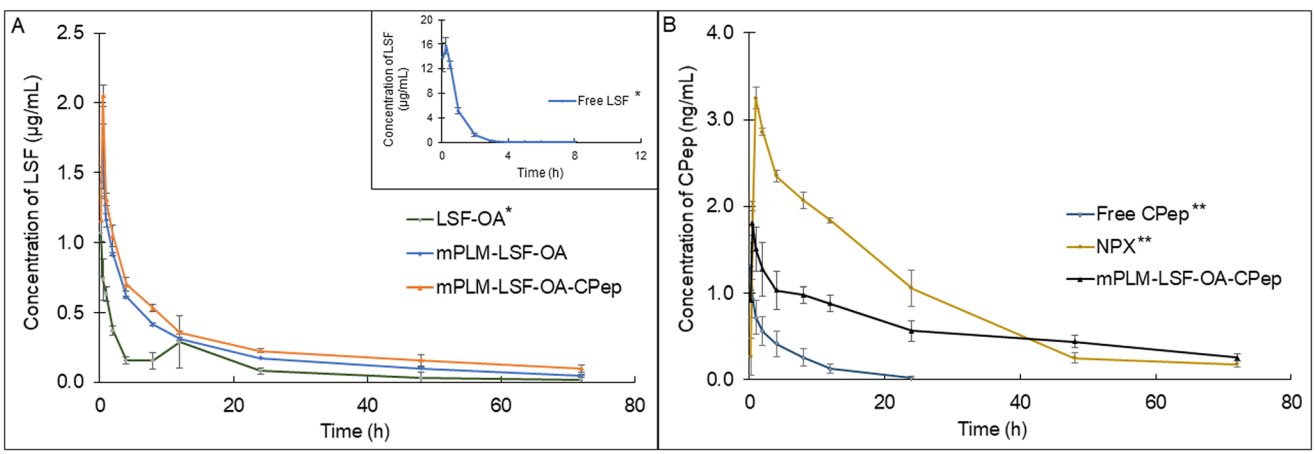

Fig. 7 Plasma-concentration time profile of (A) LSF at 15 mg kg^{-1} (~30 mg kg^{-1} of LSF-OA) dose and (B) CPep at 1 µg kg^{-1} dose after i.v. administration in Wistar rats. Each point represents mean ($n = 3$) ± SEM. *The plot of Free LSF and LSF-OA has already been published. Reprinted (adapted) with permission from {A. K. Singh, K. S.Italiya, S.Narisepalli, A. Chitkara, and A. Mittal, Role of the chain length and degree of unsaturation of fatty acids in the physicochemical and pharmacological behavior of drug–fatty acid conjugates in diabetes, *J. Med. Chem.*, 2021, **64**(19), 14217–14229. DOI: 10.1021/acs.jmedchem.1c00391}. Copyright {2021} American Chemical Society.[9] **The plot of Free CPep and NPX has already been published. Reprinted from A. K. Singh, S. A. Salunkhe, D. Chitkara, A. Mittal, Potent anti-inflammatory and anti-apoptotic activities of electrostatically complexed C-peptide nanospheres ameliorate diabetic nephropathy, *Biomater. Adv.*, **163**, 213935. DOI: 10.1016/j.bioadv.2024.213935. Copyright (2024), with permission from Elsevier.[17] Here it has been presented for comparison and clarity.

increased to 22.157 ± 1.12 h from 0.818 ± 0.06 h, as shown by free LSF. With an increase in MRT, the Cl of LSF in mPLM-LSF-OA decreased by 13 fold than LSF-OA. Additionally, LSF in the co-delivery system (mPLM-LSF-OA-CPep) demonstrated a further 2- and 1.4-fold increase in $t_{\frac{1}{2}}$ and V_d in comparison to the mPLM-LSF-OA formulation, respectively.

Also, Table 1B confirmed the improvement in PK parameters for CPep in mPLM-LSF-OA-CPep compared to the free

Table 1 Pharmacokinetic parameters of (A) LSF and (B) CPep administered in Wistar rats

(A)

Parameters	Free LSF[a]	LSF-OA micelles[a]	mPLM-LSF-OA	mPLM-LSF-OA-CPep
$t_{\frac{1}{2}}$ (h)	0.75 ± 0.03	4.44 ± 0.47	11.59 ± 0.17	23.23 ± 0.92
$AUC_{0-\infty}$ (h ng mL^{-1})	1.47 ± 5.91	6.63 ± 12.71	16.14 ± 0.35	23.17 ± 2.78
MRT (h)	0.82 ± 0.06	7.91 ± 0.93	22.17 ± 1.12	30.16 ± 2.80
V_d (mL kg^{-1})	961.55 ± 79.16	14 974.42 ± 1588.02	3108.29 ± 92.30	4370.71 ± 232.91
Cl (mL h^{-1} kg^{-1})	1020.90 ± 39.46	2415.30 ± 407.29	185.89 ± 14.21	130.68 ± 14.87

Free LSF, LSF-OA micelles, mPLM-LSF-OA and mPLM-LSF-OA-CPep (~15 mg kg^{-1} LSF; i.v.) were administered to rats and PK parameters analyzed using a non-compartmental method; mean (n = 3) ± SEM.

(B)

Parameters	Free CPep[b]	NPX[b]	mPLM-LSF-OA-CPep
$t_{\frac{1}{2}}$ (h)	3.47 ± 0.65	21.95 ± 2.63	34.06 ± 2.15
$AUC_{0-\infty}$ (h ng mL^{-1})	8.145 ± 2.65	68.09 ± 5.53	57.68 ± 1.88
MRT (h)	6.17 ± 0.76	25.90 ± 2.99	26.49 ± 0.59
V_d (mL kg^{-1})	793.05 ± 283.66	462.31 ± 17.37	899.97 ± 57.88
Cl (mL h^{-1} kg^{-1})	178.98 ± 86.33	14.87 ± 1.17	18.33 ± 0.64

Free CPep, NPX and mPLM-LSF-OA-CPep (~1 μg kg^{-1} CPep; i.v.) were administered to rats and PK parameters analyzed by non-compartmental method; mean (n = 3) ± SEM.

$t_{\frac{1}{2}}$: half-life, $AUC_{0-\infty}$: area under the curve from time 0 to last measurable concentration, MRT: mean residence time, V_d: volume of distribution, Cl: clearance, CPep: C-peptide, and NPX: CPep nano-complexes. [a] This data has already been published. Reprinted (adapted) with permission from {A. K. Singh, K. S. Italiya, S. Narisepalli, A. Chitkara and A. Mittal, Role of chain length and degree of unsaturation of fatty acids in the physicochemical and pharmacological behavior of drug–fatty acid conjugates in diabetes, *J. Med. Chem.*, 2021, **64**(19), 14217–14229. DOI: 10.1021/acs.jmedchem.1c00391}. Copyright {2021}, the American Chemical Society.[9] Here it has been presented for comparison and clarity. [b] This data has already been published. Reprinted from A. K. Singh, S. A. Salunkhe, D. Chitkara, A. Mittal, Potent anti-inflammatory and anti-apoptotic activities of electrostatically complexed C-peptide nanospheres ameliorate diabetic nephropathy, *Biomater. Adv.*, **163**, 213935. DOI: 10.1016/j.bioadv.2024.213935. Copyright (2024), with permission from Elsevier.[17] Here it has been presented for comparison and clarity.

CPep and CPep nano-complexes (NPX). In comparison to the free CPep, NPX proved to be beneficial with a 6.45-fold elevated $t_{\frac{1}{2}}$ and 12.09-fold decrease in Cl. mPLM-LSF-OA-CPep demonstrated a significant improvement in PK parameters, with a 1.55- and 1.94-fold enhanced $t_{\frac{1}{2}}$ and V_d in comparison to NPX, respectively. Hence, it is evident that mPLM-LSF-OA-CPep could improve the PK profile of both therapeutic molecules, LSF and CPep, together.

4.8 *In vivo* efficacy study

The animals underwent weekly monitoring of FGL and body weight and were sacrificed after 8 weeks. After maintenance of diabetes for one month, the animals were treated with the prepared nanoparticles according to the scheme shown in Fig. 8A. At the end of the study, the FGL of the mPLM-LSF-OA- and mPLM-LSF-OA-CPep-treated animals was measured and was found to be 447.75 ± 29.15 and 331 ± 33.33 mg dL^{-1}, which is 18.29% and 39.6% lower than that observed in the DC animals, respectively (548.75 ± 18.03 mg dL^{-1}; Fig. 8B). In general, the body weight tends to decrease during diabetes. After 8 weeks in this study, the body weight of the DC animals was found 31.39% lower than that of the NC animals. However, nanoparticle treatment contributed to a partial recovery in body weight with a 12.79% and 17.44% increase in body weight in the mPLM-LSF-OA and mPLM-LSF-OA-CPep-treated animals, respectively, in comparison to the DN animals (Fig. 8C). At the end of the 8th week of this study, the collected urine samples were analysed for nephropathy biomarkers such as creatinine and albumin, which were found to be significantly reduced after treatment with the mPLM-LSF-OA-CPep nanoparticles, that is, 4.8- and 2.4-fold compared to the DC group, as shown in Fig. 8F and G, respectively.

4.8.1 IL-6 and TNF-α cytokine estimation. The IL-6 and TNF-α signalling pathways play a crucial role in mediating the inflammatory responses that are pivotal to the progression of DN. The signalling pathways of TNF-α and IL-6 are linked to an augmented deposition of ECM within the kidneys, resulting in renal damage mediated by cytotoxic effects. In the DC animals, the levels of IL-6 and TNF-α were found to be markedly elevated (3.4 and 9.51 ng mL^{-1}) after 8 weeks of disease progression, respectively. However, these levels were significantly reduced to 1.26 and 4.63 ng mL^{-1} following treatment with mPLM-LSF-OA-CPep for 4 weeks, respectively (Fig. 8D). This reduction clearly suggests a potential delay in the progression of DN.

4.8.2 Insulin level estimation. In diabetic patients, the activation of ROS and inflammatory cytokines contributes to the depletion of pancreatic β cells. This depletion results in reduced insulin levels, ultimately leading to elevated blood glucose levels. Treatment with mPLM-LSF-OA and mPLM-LSF-OA-CPep nanoparticles significantly increased the insulin concentration by 4.9- and 6.8-fold compared to the DC animals, respectively (Fig. 8E). This effect was attributed to the protection of residual pancreatic β cells from pro-inflammatory cytokines and contributed to the control of the blood glucose level.

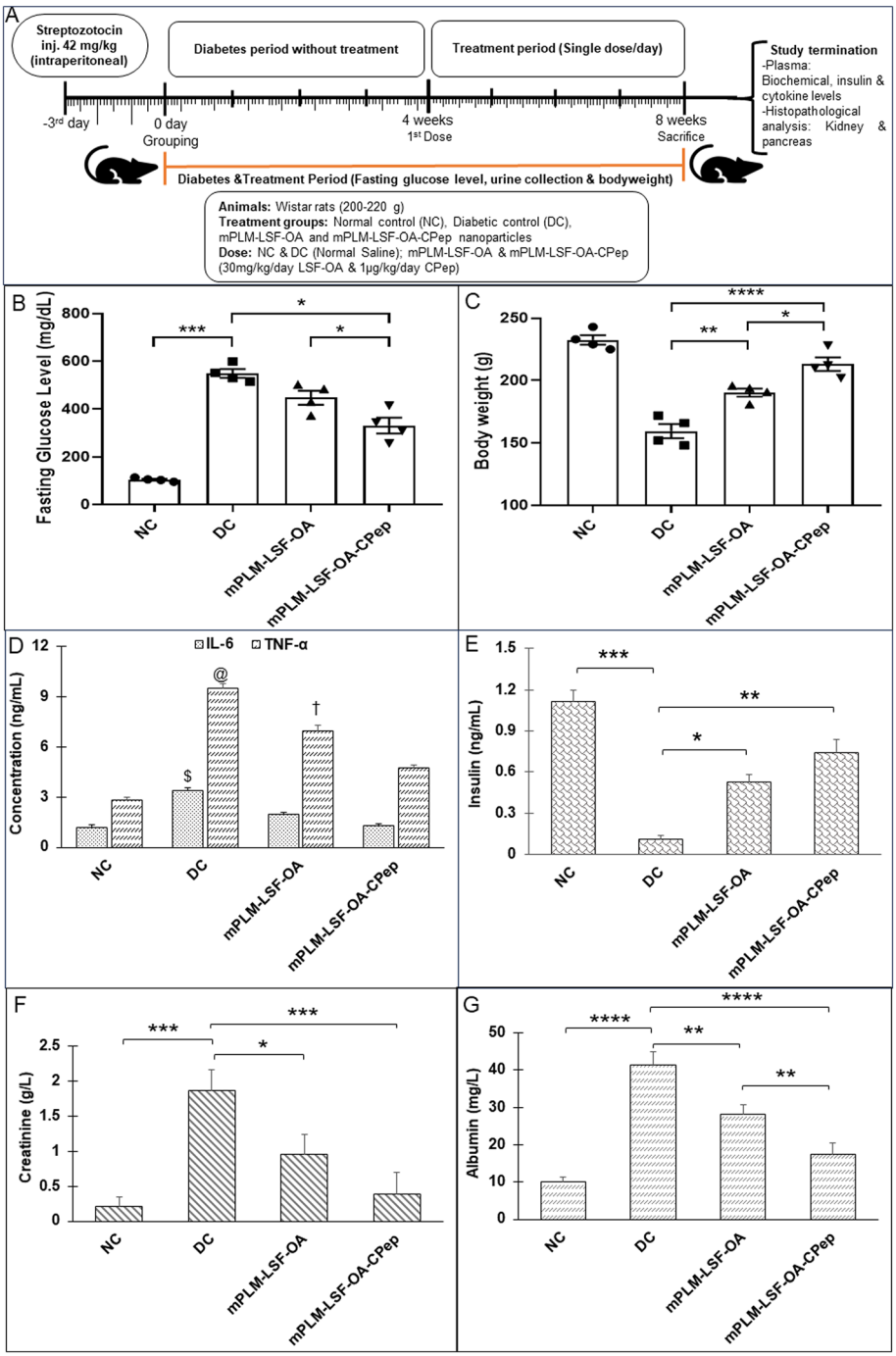

Fig. 8 *In vivo* efficacy study in STZ-induced DN animal model, parameters recorded after 8 weeks. (A) Schematic representation of *in vivo* animal study. (B) Terminal fasting blood glucose level and (C) animal body weight. *$p < 0.05$; **$p < 0.005$; ***$p < 0.0005$; ****$p < 0.0001$. (D) Inflammatory cytokine, IL-6 and TNF-α levels in plasma. $^{\$}$DC *vs.* mPLM-LSF-OA and mPLM-LSF-OA-CPep ($^{\$}p < 0.005$), $^{@}$DC *vs.* mPLM-LSF-OA-CPep ($^{@}p < 0.0001$) and, †mPLM-LSF-OA *vs.* DC and mPLM-LSF-OA-CPep ($^{\dagger}p < 0.005$). (E) Plasma insulin level. Biochemical parameters (analyzed in urine samples) (F) creatinine and (G) albumin. *$p < 0.05$; **$p < 0.005$; ***$p < 0.0005$. All data are represented as mean ($n = 4$) ± SEM. NC: normal/non-diabetic control, DC: diabetic control, and STZ: streptozotocin.

4.8.3 *In vivo* histology study

4.8.3.1 Effect on kidney. The assessment of renal environmental changes due to DN was carried out by histopathological examination of kidney sections using H&E and PAS staining. In Fig. 9A, the H&E staining of the kidney shows the glomerulus (G), distal tubule (DT), and proximal convoluted tubule (PCT) in the NC group without any pathological changes. In contrast, the DC reveals severe glomerulosclerosis, shrinkage, and depletion of the glomerulus along with tubular injury. However, the mPLM-LSF-OA- and mPLM-LSF-OA-CPep-

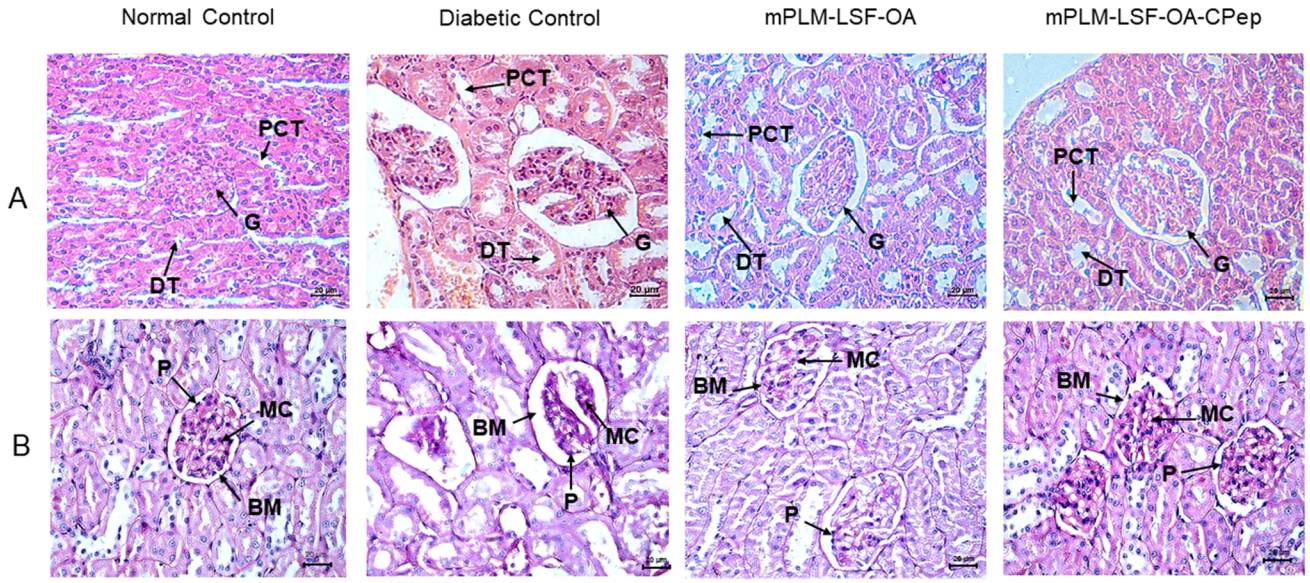

Fig. 9 Histopathological examination of kidney sections of different groups after 8 weeks of diabetes induction: (A) H&E and (B) PAS staining. Magnification 400× and scale bar 20 μm. G, glomerulus; PCT, proximal convoluted tubule; DT, distal tubule; P, podocytes; MC, mesangial cells; and BS, basement membrane.

treated groups exhibit well defined glomerular structures and improved nephron conditions. Similarly, after PAS staining, the treatment groups demonstrated reduced hypertrophy and Bowman's capsule expansion with less basement membrane (BM) space (Fig. 9B). DN is characterized by podocytes (P) and mesangial cell (MC) proliferation, together with renal tubular epithelial degeneration. Therefore, the treatment group showed reduced intracellular glycogen accumulation, diminished infiltration of inflammatory cells (seen as blue nuclei in Fig. 9B), mild mesangial expansion, less deposition of mesangial matrix, and almost normal relative glomerular basement membrane thickness, indicating the improved condition of the kidney.

4.8.3.2 Effect on pancreas. Following a 4-week treatment period for diabetic animals, the animals were euthanized, and the pancreatic Islet of Langerhans (IL) morphology was evaluated through H&E staining. In comparison to the NC animals, the rat pancreas of the DC animals exhibited a significant reduction in the number of β cells (seen as blue coloured cells in Fig. 10A) accompanied with a damaged structure. The

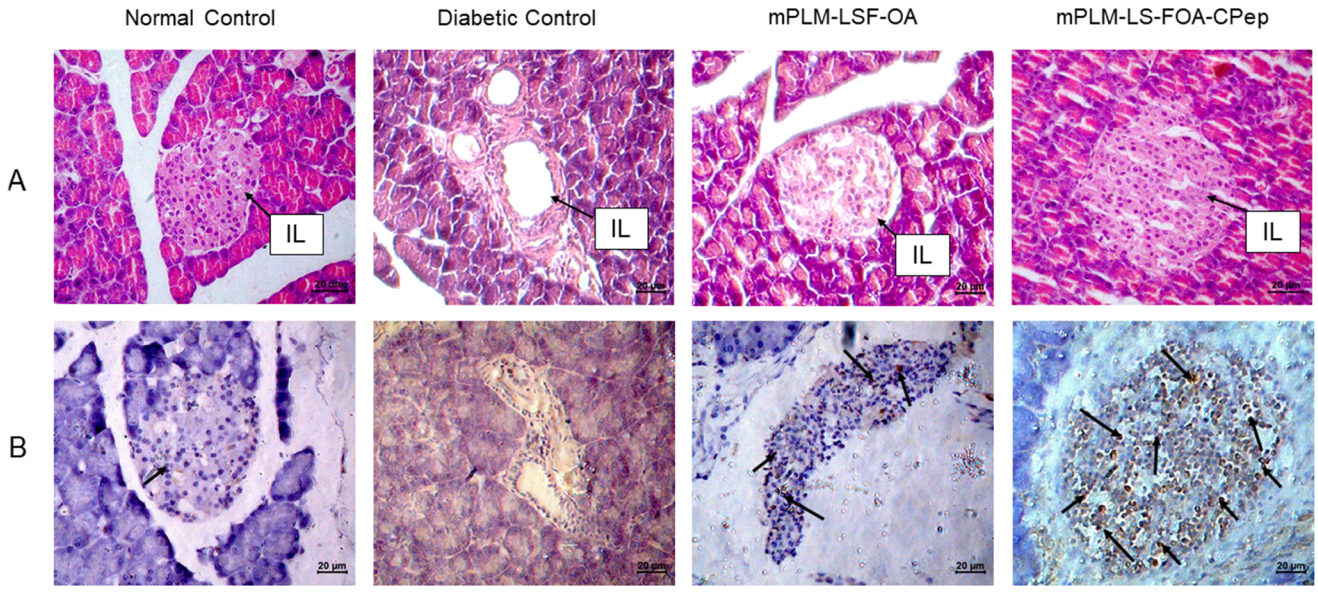

Fig. 10 Histological analysis of pancreatic sections of different groups after 4 weeks of treatment. (A) H&E staining and (B) immunohistochemical analysis of pancreatic tissue for Ki-67 expression in β cells of islets of Langerhans. Magnification 400× and scale bar 20 μm. IL: Islets of Langerhans.

depletion of β cells serves as evidence of diabetes induction and progression in animals. However, compared to the DC animals, the groups treated with mPLM-LSF-OA and mPLM-LSF-OA-CPep showed a much better-preserved islet structure (Fig. 10A).

4.9 Immunohistochemical analysis

To corroborate the findings regarding insulin secretion and pancreatic histology indicating the proliferation of pancreatic cells, the presence of intact islet structures after treatment with mPLM-LSF-OA and mPLM-LSF-OA-CPep nanoparticles justifies the existence of beta cells, subsequently leading to an increase in insulin concentration in the plasma, as seen in Fig. 8D. The proliferation marker Ki-67 was employed to stain the pancreatic tissue sections, revealing the more prominent staining of proliferative cells in the pancreatic islets in the mPLM-LSF-OA-CPep group compared to the mPLM-LSF-OA-treated group (Fig. 10B).

5. Discussion

The pathophysiology of DN is correlated with the predisposition of DM, a metabolic disorder with prominent indication of chronic hyperglycemia, which can advance to micro- and macrovascular complications in the kidney.[23] The molecular mechanism of DN involves the activation of different biological pathways, including polyol, PKC, and AGE mediated crosstalk with the overproduction of ROS, dysregulated growth factors (GFs), and abnormalities in the non-coding RNAs.[24] Generally, the therapeutic limitations of monotherapy are aggravated by pathological complexity, severity and progression of DM, which necessitate the requirement of delivering a combination of therapeutic molecules with multifaceted actions.[25] Recently, a microfluidic-based liposomal formulation was reported for the co-delivery of anti-diabetic hydrophilic and lipophilic molecules, *i.e.*, metformin and glipizide, which improved the loading efficiency of both molecules and provided 2-fold faster release than the formulation with single molecules.[26] Another niosomal formulation of glipizide and metformin hydrochloride was reported, wherein the thin film hydration approach was adopted to encapsulate the hydrophobic metformin, while the hydrophilic glipizide was loaded by simple incubation with metformin-loaded nanoparticles. The structural integrity of niosomes was ascertained by incorporation of cholesterol in the formulation.[27] These studies exemplify that co-delivery strategies are becoming a major area of focus for the treatment of DM and enable "multiple compound–multiple target approach" to achieve a reduced dose, better dosage regimen, and desirable patient compliance together with possible additive or synergistic outcome.[25]

LSF-LA polymeric micelles formulated using the film hydration method have already been reported by our group to exhibit an improved $t_{\frac{1}{2}}$ (2.79 fold) in comparison to the LSF-LA self-assembled micelles.[25,28] Recently, tannic acid-iron complex-based surface-modified PLGA nanoparticles were reported to deliver the M2 peptide (YEQDPWGVKWWY) for the selective targeting of tumor-associated M2 macrophages. The surface-modified PLGA NP complexed the peptide by simple incubation for 3 h in bicine buffer (pH 7.4).[29] In the present study, the single emulsion method was utilized to develop LSF-OA-encapsulated polymeric nanoparticles (mPLM-LSF-OA with 78.89% EE) with a surface potential of +18.3 ± 2.28 mV using the cationic mPEG-*b*-P(CB-{g-DMDP}-*co*-LA) polymer. These nanoparticles were further explored to develop a co-delivery system, mPLM-LSF-OA-CPep, wherein mPLM-LSF-OA was complexed with CPep by electrostatic interaction, resulting in the combination formulation with a particle size of 208.6 ± 7.4 nm, surface potential of +5.2 ± 2.37 mV and 82.75% CPep complexation capacity (Fig. 2A and B). The cationic charges present on the lipid or polymeric nanocarriers may damage the cells, causing cell shrinkage, reduced mitosis, endosomal disruption and vacuolization of the cytoplasm. This toxicity is generally due to the unbalanced cationic charge on their structures, wherein the groups imparting cationic charge such as quaternary ammonium amphiphiles are more toxic than their tertiary amine counterparts. Also, it has been reported that linking PEG on polyethyleneimine (PEI) polymers reduces their toxicity without affecting their gene delivery efficiency.[30,31] Herein, we utilized a PEGylated PEC polymer conjugated with small molecular weight cationic chain, which reduced the cellular toxicity, as also evident in the hemocompatibility study. There was an ~2-fold reduction observed in hemolysis by mPLM-LSF-OA-Cep (1.68%) compared to mPLM-LSF-OA (3.64%), which can be attributed to the higher surface positive charge of mPLM-LSF-OA, and within acceptable limits according to the American Society for Testing and Materials (ASTM F756-17) (Fig. 3B).[32] This also provides evidence of the complexation of CPep om the surface of mPLM-LSF-OA.[33,34] Next, the cytoprotective effect of mPLM-LSF-OA and mPLM-LSF-OA-CPep in metabolic stress-induced MIN-6 and NRK-52E cells was confirmed by the MTT assay. HG-induced metabolic stress in MIN-6 and NRK-52E is well-reported as a cell-based model for pancreatic β-cell dysfunction, hyperglycemia, and induced renotoxicity.[35,36] In this case, dextrose (100 mM) induced 34.92 ± 2.13% and 38.17 ± 0.89% cytotoxicity in the MIN-6 and NRK-52E cells, respectively, which clearly indicated the development of hyperglycemic conditions in cells. Additionally, high glucose-induced oxidative stress was confirmed by the reduction in GSH level and suppression of eNOS expression, which may further induce cytotoxicity by activating the apoptotic marker proteins such as caspases and suppressing anti-apoptotic protein, BCL-2.[37–39] The GSH level was compromised by 2.2-fold in MIN-6 and 1.9-fold in NRK-52E. Interestingly, mPLM-LSF-OA-CPep increased the GSH level by 2.06- and 1.80-fold, and mPLM-LSF-OA elevated the level by 1.62- and ~1.27-fold in the metabolic stress-induced MIN-6 and NRK-52E cells, respectively (Fig. 5A). This clearly indicated the efficiency of the combination formulation compared to mPLM-LSF-OA. While examining the effect of high glucose on eNOS-mediated nitric oxide (NO) production, the changes were measured in terms of the level of its oxidized product nitrite (NO_2^-) by the Griess reaction. In one of the

studies, high glucose could elevate the eNOS expression by 2-fold in endothelial cells, which enhanced the NO_2^- release by 40% together with ~300-fold increase in the release of superoxide. Together, NO and O_2^- resulted in the generation of a potent oxidant, peroxynitrile ($ONOO^-$), which may contribute to endothelial dysfunction in human aortic endothelial cells.[40] According to our study, the HG-treated MIN-6 and NRK-52E cells exhibited an ~9.7- and ~8.6-fold increment in NO_2^- production in comparison to the medium control group, which was found to be in agreement with the literature reports. mPLM-LSF-OA and mPLM-LSF-OA-CPep further demonstrated their efficiency by reducing NO_2^- by 1.6- and 2.3-fold in the MIN-6 cells, whereas 1.72- and 3.5-fold in NRK-52E, respectively. This observation could be correlated with the observed increase in GSH level, and interestingly, mPLM-LSF-OA-CPep was found to be more potent in reducing the oxidative stress in the cells compared to mPLM-LSF-OA in the HG-exposed cells. The oxidative and nitrosative stress led to apoptosis and necrosis in the various cells, and also triggered the reduction of GSH in HG-induced endothelial cells, leading to DNA damage.[38,41] The induction and restoration of the GSH level protected the kidney and insulinoma cells from apoptosis, wherein the nanoparticles demonstrated a significantly higher anti-apoptotic effect, as evident by the higher percentage of living cells of 92.53% and 94.82%, respectively (Fig. 6). Advanced drug delivery has opened pathways to sustain, target, dose regimen, and stabilize therapeutic molecules, and therefore CPep was PEGylated with 40 kDa PEG, covalently bound at its N-terminus and screened for neuropathy treatment. The conjugation increased the $t_{\frac{1}{2}}$ of CPep to 6–7 days without any adverse effect and marked improvement in VPT after 52 weeks of clinical trials.[15,42] The beneficial effect of the co-delivery nanosystem was also prominently seen in the PK profile of LSF and CPep when administered as mPLM-LSF-OA-CPep. Although mPLM-LSF-OA increased the $t_{\frac{1}{2}}$ of LSF by ~2.6-fold more than that of the LSF-OA self-assembled micelles, mPLM-LSF-OA-CPep enhanced the LSF $t_{\frac{1}{2}}$ to ~5.23- and 2-fold higher compared to the LSF-OA micelles and mPLM-LSF-OA, respectively.[9] Also, mPLM-LSF-OA-CPep enhanced the $t_{\frac{1}{2}}$ of CPep by ~1.55-fold than that of NPX (Table 1). This clearly highlighted the improved potential of the co-delivery system in comparison to the monotherapy formulations. The synchronized improvement in the PK profile of a combination of active molecules through nanoformulation is also well reported in the case of the silica nanoformulation of the CDK4/6 inhibitor palbociclib and the autophagy inhibitor hydroxychloroquine in the treatment of pancreatic cancer.[43]

Besides synthesizing the novel molecule LSF, Nadler *et al.* also explored this small molecule in combination with exendin-4, which was delivered *via* an Alzet osmotic mini-pump, providing the dual effect of supressing autoimmune cytokines and enhancing the proliferation of β-cells to reverse T1DM in a mouse model. It was found that the combination successfully reversed hyperglycemia within a week of starting the treatment and maintained glucose for more than 3 months, which was attributed to the recovered insulin secretion, and restored other hormonal levels. Although LSF alone stabilised FGL in some mice, exendin-4 alone could not improve hyperglycemia, and therefore the combination played a pivotal role in the treatment of T1DM.[10,44,45] Previously, our group reported the therapeutic efficacy of LSF-OA as an anti-diabetic, anti-inflammatory and anti-oxidant molecule in T1DM.[9] CPep also exhibits anti-oxidant, anti-apoptotic, anti-inflammatory and reno-protectivity activity in the treatment of diabetes and its complications.[12] Herein, the efficacy of the co-delivery formulation was confirmed in the STZ-induced DN animal model. The observed reduction in the FGL level and ~6.7-fold elevated insulin level in comparison to the DN group indicated the efficacy of the co-delivery nanosystem. The observed anti-diabetic effect with enhanced insulin level is attributed to the pancreatic β-cell protection and ability of LSF to induce the proliferation of pancreatic cells, as reported in the literature.[6,46] As indicated in Fig. 8C and D, mPLM-LSF-OA-CPep-treated animals demonstrated an ~2.69- and 2.05-fold reduction in proinflammatory cytokines (IL-6 and TNF-α), while mPLM-LSF-OA exhibited an ~1.76- and 1.37-fold reduction in the aforementioned cytokines levels in comparison to the DN control group, respectively. This clearly indicated the superior anti-inflammatory activity of the combination nano-formulation in comparison to mPLM-LSF-OA, which is attributed to the presence of the anti-inflammatory and renoprotective molecule CPep together with LSF-OA.[47] Also, H&E and PAS staining of the kidney sections demonstrated reduced intracellular glycogen accumulation, diminished infiltration of inflammatory cells, mild mesangial expansion, less deposition of mesangial matrix, and almost normal relative glomerular basement membrane thickness upon treatment with the combination formulation for 4 weeks. Ki-67 staining of the pancreas, a marker of proliferation, in the different groups also indicated that the cellular proliferation in the mPLM-LSF-OA-CPep-treated animals was much better than that in the other groups (Fig. 10B).[48] These studies demonstrate the potential of mPLM-LSF-OA-CPep to provide an effective delivery system for the small molecule drug LSF and peptide CPep together with harnessing their synergistic effect in the treatment of the DN, which was evidently higher in comparison to their monotherapy formulations, *i.e.*, mPLM-LSF-OA and NPX, respectively.

6. Conclusion

Herein, we investigated a co-delivery strategy to harness the potential benefits of LSF and CPep in treating DN. It is noteworthy to mention that the combined therapy involving CPep and the anti-inflammatory small molecule drug LSF has not been explored to date, neither in terms of its effectiveness in treating DN nor for the development of a formulation. The clinical indication for the formulation developed in this work is the early diagnosis of diabetes, which can become chronic if left untreated and develop into a long-term metabolic disorder. LSF and C-peptide are envisioned to initially serve as anti-inflammatory and antioxidant agents, preventing the

depletion of pancreatic cells and decreasing the unbalanced ROS levels, thereby controlling the blood glucose levels and maintaining kidney functionality. The therapy needs to be further continued daily given that diabetes progresses to the chronic stage. In this case, the combination therapy with C-pep and LSF would help restore the kidney cells, increase the antioxidant-like GSH levels, decrease the pro-inflammatory cytokine and ROS levels, and regenerate pancreatic β-cells, thereby restoring the insulin levels in the body. Hence, this study highlighted the potential synergistic effects and enhanced therapeutic efficacy of this combination approach for the treatment of DN.

Author contributions

Arihant Kumar Singh: formal analysis, investigation, experiments, data curation, writing-original draft. Kommera Sai Pradyuth: investigation and data curation. Deepak Chitkara: reviewed and edited the manuscript. Anupama Mittal: project administration, supervision, methodology, resources, writing, review & editing of manuscript.

Data availability

Data shall be made available upon genuine request to the authors.

Conflicts of interest

The authors declare that they have no known competing financial interests or personal relationships that could have appeared to influence the work reported in this paper. An Indian patent application has been filed on this work (# 202311047523).

References

1 K. Ogurtsova, L. Guariguata, N. C. Barengo, P. L.-D. Ruiz, J. W. Sacre, S. Karuranga, H. Sun, E. J. Boyko and D. J. Magliano, IDF diabetes Atlas: Global estimates of undiagnosed diabetes in adults for 2021, *Diabetes Res. Clin. Pract.*, 2022, **183**, 109118.
2 A. D. Association, Diagnosis and classification of diabetes mellitus, *Diabetes Care*, 2014, **37**(Supplement_1), S81–S90.
3 L. Chen, D. J. Magliano and P. Z. Zimmet, The worldwide epidemiology of type 2 diabetes mellitus—present and future perspectives, *Nat. Rev. Endocrinol.*, 2012, **8**(4), 228–236.
4 B. Lin, Y.-Y. Ma and J.-W. Wang, Nano-technological approaches for targeting kidney diseases with focus on diabetic nephropathy: recent progress, and future perspectives, *Front. Bioeng. Biotechnol.*, 2022, **10**, 870049.
5 Z. Yang, M. Chen and J. L. Nadler, Lisofylline: a potential lead for the treatment of diabetes, *Biochem. Pharmacol.*, 2005, **69**(1), 1–5.
6 J. S. Striffler and J. L. Nadler, Lisofylline, a novel anti-inflammatory agent, enhances glucose-stimulated insulin secretion in vivo and in vitro: studies in prediabetic and normal rats, *Metabolism*, 2004, **53**(3), 290–296.
7 K. S. Italiya, S. Mazumdar, S. Sharma, D. Chitkara, R. I. Mahato and A. Mittal, Self-assembling lisofylline-fatty acid conjugate for effective treatment of diabetes mellitus, *Nanomedicine*, 2019, **15**(1), 175–187.
8 J. A. Lillibridge, T. F. Kalhorn and J. T. Slattery, Metabolism of lisofylline and pentoxifylline in human liver microsomes and cytosol, *Drug Metab. Dispos.*, 1996, **24**(11), 1174–1179.
9 A. K. Singh, K. S. Italiya, S. Narisepalli, D. Chitkara and A. Mittal, Role of chain length and degree of unsaturation of fatty acids in the physicochemical and pharmacological behavior of drug–fatty acid conjugates in diabetes, *J. Med. Chem.*, 2021, **64**(19), 14217–14229.
10 Z. Yang, M. Chen, J. D. Carter, C. S. Nunemaker, J. C. Garmey, S. D. Kimble and J. L. Nadler, Combined treatment with lisofylline and exendin-4 reverses autoimmune diabetes, *Biochem. Biophys. Res. Commun.*, 2006, **344**(3), 1017–1022.
11 J. A. Shaw, P. Shetty, K. D. Burns, D. Fergusson and G. A. Knoll, C-peptide as a therapy for kidney disease: A systematic review and meta-analysis, *PLoS One*, 2015, **10**(5), e0127439.
12 J. Chen, Y. Huang, C. Liu, J. Chi, Y. Wang and L. Xu, The role of C-peptide in diabetes and its complications: an updated review, *Front. Endocrinol.*, 2023, **14**, 1256093.
13 N. Zashikhina, V. Sharoyko, M. Antipchik, I. Tarasenko, Y. Anufrikov, A. Lavrentieva, T. Tennikova and E. Korzhikova-Vlakh, Novel formulations of C-peptide with long-acting therapeutic potential for treatment of diabetic complications, *Pharmaceutics*, 2019, **11**(1), 27.
14 S. H. Jung, J. Y. Lee, S. H. Lee, M. H. Kwon, E. T. Han, W. S. Park, S. H. Hong, Y. M. Kim and K. S. Ha, Preventive Effects of Thermosensitive Biopolymer–Conjugated C–Peptide against High Glucose–Induced Endothelial Cell Dysfunction, *Macromol. Biosci.*, 2019, **19**(9), 1900129.
15 J. Wahren, H. Foyt, M. Daniels and J. C. Arezzo, Long-acting C-peptide and neuropathy in type 1 diabetes: a 12-month clinical trial, *Diabetes Care*, 2016, **39**(4), 596–602.
16 A.-J. Lee, Y.-J. Lee, H.-Y. Jeon, M. Kim, E.-T. Han, W. S. Park, S.-H. Hong, Y.-M. Kim and K.-S. Ha, Application of elastin-like biopolymer-conjugated C-peptide hydrogel for systemic long-term delivery against diabetic aortic dysfunction, *Acta Biomater.*, 2020, **118**, 32–43.
17 A. K. Singh, S. A. Salunkhe, D. Chitkara and A. Mittal, Potent anti-inflammatory and anti-apoptotic activities of electrostatically complexed C-peptide nanospheres ameliorate diabetic nephropathy, *Biomater. Adv.*, 2024, **163**, 213935.
18 K. S. Italiya, S. Mazumdar, S. Sharma, D. Chitkara, R. I. Mahato and A. Mittal, Self-assembling lisofylline-fatty acid conjugate for effective treatment of diabetes mellitus, *Nanomedicine*, 2019, **15**(1), 175–187.

19 S. Sharma, S. Mazumdar, K. S. Italiya, T. Date, R. I. Mahato, A. Mittal and D. Chitkara, Cholesterol and morpholine grafted cationic amphiphilic copolymers for miRNA-34a delivery, *Mol. Pharm.*, 2018, **15**(6), 2391–2402.
20 K. S. Italiya, M. Basak, S. Mazumdar, D. K. Sahel, R. Shrivastava, D. Chitkara and A. Mittal, Scalable self-assembling micellar system for enhanced oral bioavailability and efficacy of lisofylline for treatment of type-I diabetes, *Mol. Pharm.*, 2019, **16**(12), 4954–4967.
21 O. Boscolo, S. Flor, L. Salvo, C. Dobrecky, C. Höcht, V. Tripodi, M. Moretton and S. Lucangioli, Formulation and Characterization of Ursodeoxycholic Acid Nanosuspension Based on Bottom-Up Technology and Box–Behnken Design Optimization, *Pharmaceutics*, 2023, **15**(8), 2037.
22 A. Mittal, D. Chitkara, S. W. Behrman and R. I. Mahato, Efficacy of gemcitabine conjugated and miRNA-205 complexed micelles for treatment of advanced pancreatic cancer, *Biomaterials*, 2014, **35**(25), 7077–7087.
23 N. M. Selby and M. W. Taal, An updated overview of diabetic nephropathy: Diagnosis, prognosis, treatment goals and latest guidelines, *Diabetes, Obes. Metab.*, 2020, **22**, 3–15.
24 S. Paul, A. Ali and R. Katare, Molecular complexities underlying the vascular complications of diabetes mellitus–A comprehensive review, *J. Diabetes Its Complications*, 2020, **34**(8), 107613.
25 Q. Gao, J. Feng, W. Liu, C. Wen, Y. Wu, Q. Liao, L. Zou, X. Sui, T. Xie and J. Zhang, Opportunities and challenges for co-delivery nanomedicines based on combination of phytochemicals with chemotherapeutic drugs in cancer treatment, *Adv. Drug Delivery Rev.*, 2022, 114445.
26 S. Joshi, M. T. Hussain, C. B. Roces, G. Anderluzzi, E. Kastner, S. Salmaso, D. J. Kirby and Y. Perrie, Microfluidics based manufacture of liposomes simultaneously entrapping hydrophilic and lipophilic drugs, *Int. J. Pharm.*, 2016, **514**(1), 160–168.
27 N. Samed, V. Sharma and A. Sundaramurthy, Hydrogen bonded niosomes for encapsulation and release of hydrophilic and hydrophobic anti-diabetic drugs: an efficient system for oral anti-diabetic formulation, *Appl. Surf. Sci.*, 2018, **449**, 567–573.
28 K. S. Italiya, A. K. Singh, D. Chitkara and A. Mittal, Nanoparticulate tablet dosage form of lisofylline-linoleic acid conjugate for type 1 diabetes: in situ single-pass intestinal perfusion (SPIP) studies and pharmacokinetics in rat, *AAPS PharmSciTech*, 2021, **22**, 1–12.
29 L. Pang, Y. Pei, G. Uzunalli, H. Hyun, L. T. Lyle and Y. Yeo, Surface modification of polymeric nanoparticles with M2pep peptide for drug delivery to tumor-associated macrophages, *Pharm. Res.*, 2019, **36**, 1–12.
30 H. Lv, S. Zhang, B. Wang, S. Cui and J. Yan, Toxicity of cationic lipids and cationic polymers in gene delivery, *J. Controlled Release*, 2006, **114**(1), 100–109.
31 A. M. Weiss, M. A. Lopez, B. W. Rawe, S. Manna, Q. Chen, E. J. Mulder, S. J. Rowan and A. P. Esser-Kahn, Understanding How Cationic Polymers' Properties Inform Toxic or Immunogenic Responses via Parametric Analysis, *Macromolecules*, 2023, **56**(18), 7286–7299.
32 F. ASTM, F756-08, *Standard Practice for Assessment of Hemolytic Properties of Materials*, ASTM International, West Conshohocken, PA, ASTM Book of Standards, 2013.
33 R. F. Pagels and R. K. Prud'Homme, Polymeric nanoparticles and microparticles for the delivery of peptides, biologics, and soluble therapeutics, *J. Controlled Release*, 2015, **219**, 519–535.
34 C. Wang, S. Feng, J. Qie, X. Wei, H. Yan and K. Liu, Polyion complexes of a cationic antimicrobial peptide as a potential systemically administered antibiotic, *Int. J. Pharm.*, 2019, **554**, 284–291.
35 L. Lv, X. Wang, J. Shen, Y. Cao and Q. Zhang, MiR-574-3p inhibits glucose toxicity-induced pancreatic β-cell dysfunction by suppressing PRMT1, *Diabetol. Metab. Syndr.*, 2022, **14**(1), 1–11.
36 M. F. Khan, A. Mathur, V. K. Pandey and P. Kakkar, Naringenin alleviates hyperglycemia-induced renal toxicity by regulating activating transcription factor 4–C/EBP homologous protein mediated apoptosis, *J. Cell Commun. Signaling*, 2021, 1–21.
37 X. Liu, S. Han, Y. Yang, J. Kang and J. Wu, Glucose-induced glutathione reduction in mitochondria is involved in the first phase of pancreatic β-cell insulin secretion, *Biochem. Biophys. Res. Commun.*, 2015, **464**(3), 730–736.
38 D. A. Allen, M. M. Yaqoob and S. M. Harwood, Mechanisms of high glucose-induced apoptosis and its relationship to diabetic complications, *J. Nutr. Biochem.*, 2005, **16**(12), 705–713.
39 I. P. Salt, V. A. Morrow, F. M. Brandie, J. M. Connell and J. R. Petrie, High glucose inhibits insulin-stimulated nitric oxide production without reducing endothelial nitric-oxide synthase Ser1177 phosphorylation in human aortic endothelial cells, *J. Biol. Chem.*, 2003, **278**(21), 18791–18797.
40 F. Cosentino, K. Hishikawa, Z. S. Katusic and T. F. Lüscher, High glucose increases nitric oxide synthase expression and superoxide anion generation in human aortic endothelial cells, *Circulation*, 1997, **96**(1), 25–28.
41 L. A. Powell, S. M. Nally, D. McMaster, M. A. Catherwood and E. R. Trimble, Restoration of glutathione levels in vascular smooth muscle cells exposed to high glucose conditions, *Free Radicals Biol. Med.*, 2001, **31**(10), 1149–1155.
42 H. Foyt, M. Daniels, M. Milad and J. Wahren, Pharmacokinetics, safety, and tolerability of a long-acting C-peptide (CBX129801) in patients with type 1 diabetes, *Diabetologia*, 2012, **55**(Suppl 1), S455.
43 Y. Ji, X. Liu, J. Li, X. Xie, M. Huang, J. Jiang, Y.-P. Liao, T. Donahue and H. Meng, Use of ratiometrically designed nanocarrier targeting CDK4/6 and autophagy pathways for effective pancreatic cancer treatment, *Nat. Commun.*, 2020, **11**(1), 4249.
44 Z. Yang, M. Chen, L. B. Fialkow, J. D. Ellett, R. Wu and J. L. Nadler, The novel anti-inflammatory compound, liso-

fylline, prevents diabetes in multiple low-dose streptozotocin-treated mice, *Pancreas*, 2003, **26**(4), e99–e104.

45 G. Xu, D. A. Stoffers, J. F. Habener and S. Bonner-Weir, Exendin-4 stimulates both beta-cell replication and neogenesis, resulting in increased beta-cell mass and improved glucose tolerance in diabetic rats, *Diabetes*, 1999, **48**(12), 2270–2276.

46 M. Chen, Z. Yang, R. Wu and J. L. Nadler, Lisofylline, a novel antiinflammatory agent, protects pancreatic β-cells from proinflammatory cytokine damage by promoting mitochondrial metabolism, *Endocrinology*, 2002, **143**(6), 2341–2348.

47 J. Wahren, Å. Kallas and A. A. Sima, The clinical potential of C-peptide replacement in type 1 diabetes, *Diabetes*, 2012, **61**(4), 761–772.

48 J.-K. Yi, Z.-Y. Ryoo, J.-J. Ha, D.-Y. Oh, M.-O. Kim and S.-H. Kim, Beneficial effects of 6-shogaol on hyperglycemia, islet morphology and apoptosis in some tissues of streptozotocin-induced diabetic mice, *Diabetol. Metab. Syndr.*, 2019, **11**(1), 1–13.